PCCP

PAPER

View Article Online
View Journal | View Issue

Cite this: *Phys. Chem. Chem. Phys.*, 2015, **17**, 27894

Received 7th August 2015,
Accepted 17th September 2015

DOI: 10.1039/c5cp04676a

www.rsc.org/pccp

Gas sorption in solid surfaces: a computational study using rigid and Einstein-solid models

Mayra Lara-Peña[a] and Hector Domínguez*[b]

The reactive Monte Carlo (RxMC) method was proposed to describe the sorption of gases in solid materials due to the chemical reaction A + B ⇌ C. Two models were used to simulate the solid; the first model considered simulations with rigid particles in the solid whereas in the second model the particles were allowed to vibrate inside the solid with a given spring constant, *i.e.* an Einstein solid was used to simulate the substrate. In both models not only physisorption but also chemisorption of the fluid was observed. Sorption curves, at different spring constants, were simulated and it was noted that sorption was always enhanced with the Einstein solid model. Moreover, an inverse dependent function of the spring constant with the temperature was found. Finally, the second model might be used to explain the unusual sorption behavior observed in actual experimental reactions such as $CO_2 + Li_2O \rightleftharpoons Li_2CO_3$.

1 Introduction

Nowadays the efforts to control gas emissions due to all the environmental problems caused by carbon dioxide (CO_2) production are well known. In fact, several studies have been conducted to create new materials with good sorption properties[1–5] to retain gases. In particular, earlier studies have found that lithium ceramics present good CO_2 sorption at high temperatures.[2,6,7] In fact, it has been observed that the reaction $Li_2O + CO_2 \rightleftharpoons Li_2CO_3$ is a good process to capture CO_2, *i.e.* Li_2O (lithium oxide) is highly reactive with CO_2 to form Li_2CO_3 (lithium carbonate). Therefore, few experiments have been conducted to study such reaction and some authors, based on SEM (scanning electron microscopy) sorption data, have proposed a schematic view of how CO_2 is chemisorbed in Li_2O ceramics. They suggested that CO_2 sorption starts at the Li_2O surface by producing a Li_2CO_3 shell on the ceramic substrate. Then, at high temperatures the shell cracks creating free paths where CO_2 might diffuse inside the ceramics to react with new Li_2O and then, chemisorption suddenly increases.[2]

From the theoretical point of view CO_2 sorption has been studied by density functional theories[8–10] and by molecular simulations.[11–18] Density functional calculations (DFT-MD) might be the most fundamental approach to investigate chemical reactions by studying electronic structural transformations to include covalently bonded sites. Therefore, the methods should include reactive potentials which allow bond breaking and bond formation in the calculations such as the ReaxFF force field.[8] However, those simulations can be very expensive, so they have limitations in the system size and simulation times compared with classical methods. On the other hand, if we are interested in equilibrium states (not in the electronic structure or accurate bond interactions) it is possible to look at the energy difference only between the reactants and the products in the reaction.[18] Therefore, the reaction events (forward and reverse) can be described with classical potentials which can give us information about chemical reaction equilibria. In fact, classical molecular simulations have been employed to investigate gas adsorption in solid surfaces by using different approaches.[18–20] However, to the best of our knowledge Reactive Monte Carlo (RxMC) methods have not been used to study these kinds of systems. Therefore, in this paper computer simulations, using the RxMC method, were conducted to investigate the physics behind the reactions in solids and the mechanism of how gas sorption in solid surfaces occurs in real experiments.

In particular, we studied the reaction A + B ⇌ C as a model to understand sorption of CO_2 in surfaces of actual reactions such as $Li_2O + CO_2 \rightleftharpoons Li_2CO_3$. Moreover, a computational model, with solid surfaces composed of vibrational particles, was proposed by showing good agreement with experimental tendencies.

2 Computational method and model

The studies of gas sorption in solid surfaces were conducted by deposition of fluid particles between two parallel walls separated by a distance H. As stated before, to mimic an experimental real reaction, a simple model was simulated by considering the reaction A + B ⇌ C. In the simulations species "A", "B" and

[a] *Posgrado en Ciencias Físicas, Universidad Nacional Autónoma de México, México, D.F. 04510, Mexico*

[b] *Instituto de Investigaciones en Materiales, Universidad Nacional Autónoma de México, México, D.F. 04510, Mexico. E-mail: hectordc@unam.mx*

"C" were modeled as spherical particles and all interactions between the different species were given by a shifted Lennard-Jones potential (LJ)

$$u(r_{ij}) = 4\varepsilon_{ij}\left[\left(\frac{\sigma_{ij}}{r_{ij}}\right)^{12} - \left(\frac{\sigma_{ij}}{r_{ij}}\right)^{6}\right] \quad (1)$$

where σ_{ij} and ε_{ij} are the Lennard-Jones parameters. In the present simulations the LJ parameters of species "A", "B" and "C" were chosen to mimic CO_2, Li_2O and Li_2CO_3 molecules, respectively. The CO_2 LJ parameters were taken from the literature (ε_A/K = 236.1 K, σ_A = 3.75 Å)[21] whereas the Li_2O and Li_2CO_3 parameters were estimated by adding the LJ curves of Li, O and C (with the LJ parameters given in the literature[22,23]). Then, the LJ parameters were found by the best fitting of the resulting potential curve and ε_B/K = 84.2 K, σ_B = 2.931 Å, ε_C/K = 265.88 K, σ_B = 2.932 Å (K the Boltzmann constant) were obtained. The cross interactions were handled using the usual Lorentz–Berthelot mixing rules.

The initial configuration started from a random number of particles "A" located in a simulation box with low density ($\rho\sigma_A^3$ = 0.0245) in contact with two structured parallel solid walls. In fact, the walls were prepared with an atomistic model in a simple cubic array, with six layers, of particles type "B".

Explicit details of the reactive Monte Carlo (RxMC) method can be found in the literature[24] and we just mention the principal steps for the present simulations.

(1) A particle "A" is chosen at random and a change in position with the standard MC probability is attempted.[25]

(2) Forward reaction. A particle "B" is chosen at random and it is changed to particle "C", at the same time a particle "A" is removed from the system. Then, the move is accepted with probability of min[1, $P^{+}_{r\to s}$].

(3) Reverse reaction. A particle "C" is chosen at random and it is changed to particle "B"; at the same time a particle "A" is randomly created in the gas phase. Then, the move is accepted with a probability of min[1, $P^{-}_{s\to r}$].

Here, the transition probability for a reaction in the direction r → s is given by the following equation,

$$P_{r\to s} = e^{-\beta\delta U_{rs}}\prod_{i=1}^{n} q_i^{\nu_i}\prod_{i=1}^{n}\frac{N_i!}{[N_i+\nu_i]!} \quad (2)$$

$\beta = 1/KT$ (K the Boltzmann constant and T the temperature), δU_{rs} is the energy change from state r to s, q_i is the partition function, N_i is the number of particles of type i, ν_i is the stoichiometric coefficient of component i and n is the number of components.[24] The transition probability for the reverse reaction (s → r) can be generated by replacing ν_i by $-\nu_i$. From the chemical equilibrium conditions ($\mu_C - \mu_A - \mu_B = 0$) the transition probabilities, for the present reaction, in eqn (2) are written as

$$P^{+}_{A+B\to C} = \frac{q_C}{q_A q_B}\frac{N_A N_B}{N_C+1}e^{-\beta\delta U} \quad (3)$$

and the reverse reaction,

$$P^{-}_{C\to A+B} = \frac{q_A q_B}{q_C}\frac{N_C}{(N_A+1)(N_B+1)}e^{-\beta\delta U'} \quad (4)$$

In the last equation, q_A, q_B and q_C are the individual partition functions which have the contributions of all degrees of freedom, for instance $q_A = q_{t_A}q_{v_A}q_{r_A}$ with q_{t_A} the translational contribution, q_{v_A} the vibrational contribution and q_{r_A} includes the rotational, electrical and nuclear contributions. In our model the q_{r_i} are considered as unity whereas only particles of type "A" (the gas) present translations and the translational function is written as,

$$q_{t_A} = V\left(\frac{2\pi m_i KT}{h^2}\right)^{3/2} \quad (5)$$

with V the volume, h the constant of Planck and m the mass. Then, the transition probabilities are

$$P^{+}_{A+B\to C} = \frac{V^{*-1}T^{*-3/2}}{\Lambda}\frac{N_A N_B}{N_C+1}e^{-\delta U^*/T^*}\left(\frac{q_{v_C}}{q_{v_B}}\right) \quad (6)$$

$$P^{-}_{C\to A+B} = V^*T^{*3/2}\Lambda\frac{N_C}{(N_A+1)(N_B+1)}e^{-\delta U'^*/T^*}\left(\frac{q_{v_B}}{q_{v_C}}\right) \quad (7)$$

where the usual reduced units were used, *i.e.* $V^* = V/\sigma_A^3$, $T^* = KT/\varepsilon_A$, $U^* = U/\varepsilon_A$ and with

$$\Lambda = \left(\frac{2\pi m_A\varepsilon_A\sigma_A^2}{h^2}\right)^{3/2} \quad (8)$$

For the solid particles two wall models were simulated. In the first case the atoms in the solid were considered rigid whereas in the second case the atoms were allowed to vibrate around their equilibrium positions as simple harmonic oscillators, *i.e.* it was considered the Einstein solid model. Then, in the first model there was no vibrational partition function of particles "B" or "C", *i.e.* $q_{v_B} = q_{v_C} = 1$. For the second model the vibrational partition function, of particles "B" and "C", was written as $q_v = \sum_n e^{-\beta E_n}$ with $E_n = \hbar\omega(n + 1/2)$ where $\hbar = h/2\pi$ and ω the particle frequency.[26]

With the approximation $KT \gg \hbar\omega$, the partition functions can be written as $q_{v_B} \approx KT/\hbar\omega_B$ and $q_{v_C} \approx KT/\hbar\omega_C$. By using the relation $\omega_i = \sqrt{k_i/m_i}$ (k_i, the spring constant) eqn (6) and (7) can be rewritten as,

$$P^{+}_{A+B\to C} = \frac{V^{*-1}T^{*-3/2}}{\Lambda}\frac{N_A N_B}{N_C+1}e^{-\beta\delta U}\left(\frac{k_B m_C}{k_C m_B}\right)^{3/2} \quad (9)$$

$$P^{-}_{C\to A+B} = V^*T^{*3/2}\Lambda\frac{N_C}{(N_A+1)(N_B+1)}e^{-\beta\delta U'}\left(\frac{k_C m_B}{k_B m_C}\right)^{3/2} \quad (10)$$

were k_B and k_C are the spring constants of particles "B" and "C", respectively. Eqn (6) and (7) were used for the rigid model (with $q_{v_A} = q_{v_B} = 1$) whereas eqn (9) and (10) were used for the Einstein solid model. It is important to note that eqn (9) and (10) cannot be used for zero spring constants since they will be undefined.

All simulations were conducted in the *NVT* ensemble in a box of dimensions $X = Y = 9.0281$ and $Z = 600$ and they started with 1200 particles of type "A" and 1452 particles of type "B". Periodic boundary conditions were used in the X–Y directions only and a cutoff radius of $4.0\sigma_A$ was used. In order to keep the

solid layer structure the particles in the walls were allowed to move in X–Y directions only. Typical simulations considered runs of 10 000 MC steps for equilibration and another 50 000 MC steps (or until energy did not change significantly) for data production. Configurational energy was monitored during the simulations to determine when the systems reached equilibrium (when energy did not have significant variations). For the rest of the paper all quantities are given in reduced units and they are written without the superindex.

3 Results and discussion

3.1 Sorption

The initial simulations were conducted for the first wall model, *i.e.* the rigid model. In Fig. 1 the chemisorption of particles "A" in the solid as a function of the parameter $1/\Lambda$ (eqn (8)) is plotted for two different reduced temperatures, T = 1.69 and T = 2.96. Λ depends on the Lennard-Jones parameters, σ and ε, then a change in that variable somehow modifies the interactions between particles and consequently sorption in the substrate. In fact, it is observed from Fig. 1 that sorption decreases as the parameter $1/\Lambda$ approaches zero, *i.e.* for very large values of Λ. However, Λ cannot increase indefinitely since it will indicate that the LJ parameters will also increase indefinitely which is not physically possible. The maximum Λ value is determined by the given LJ parameters, σ and ε (previous section). Then, even when $1/\Lambda$ could be small it cannot be zero. The sorption was measured as the percentage of gain mass in the solid, $\Gamma = m_f/m_i$, where m_f and m_i are the total final and initial masses in the solid. It was observed that both temperatures produced similar sorption behavior. In fact for $1/\Lambda$ less than 2000 the gas molecules were rapidly sorbed and for higher values the sorption did not present significant variations.

Interesting was the behavior of the chemisorption as a function of the temperature. In Fig. 2 the results of those simulations are shown, for Λ = 0.0002, in the plateau region,

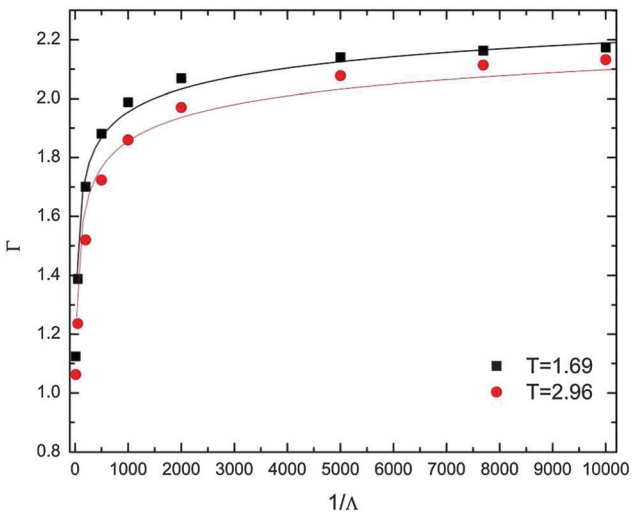

Fig. 1 Sorption curves, Γ, as a function of the parameter $1/\Lambda$ at different temperatures. The solid lines are given as a guide for the eye.

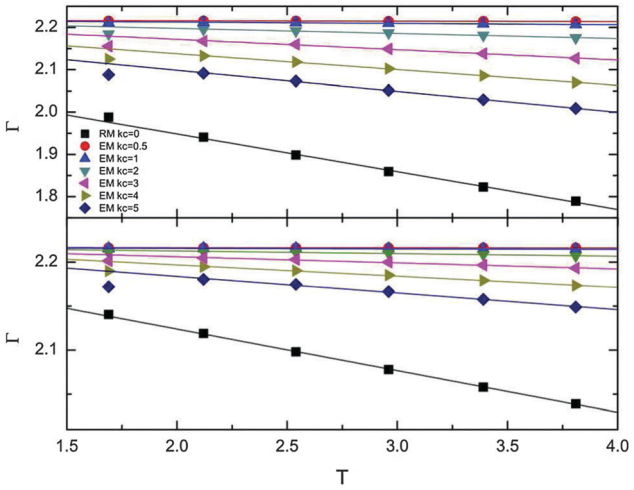

Fig. 2 Sorption curves as a function of the temperature for different k_C. Top figure for Λ = 0.001 and bottom figure for Λ = 0.0002. The solid lines are the best fitting curves to the last five points for each k_C. Data with k_C = 0 are calculated with the rigid model (RM) whereas the other k_C were calculated using the Einstein model (EM).

and Λ = 0.001, in the curvature region (see Fig. 1). Since the critical temperature for a Lennard-Jones fluid is around T = 1.25,[27] the temperatures above 1.5 were only considered to guarantee that the system was above any two phase region. For both Λ, the same behavior was observed, *i.e.* the chemisorption decreased as the temperature increased (black data in Fig. 2); however, higher sorption for Λ = 0.0002 than for Λ = 0.001 was noted at the same temperature.

All above simulations were conducted for a solid composed of rigid particles; however, when simulations were carried out using the second model, *i.e.* the Einstein solid model, different features were depicted. For those simulations different spring constants ratios, k_B/k_C, in eqn (9) and (10) were used. k_B was fixed at a value of 5 whereas k_C was changing. In the same Fig. 2 the results for different k_B/k_C ratios are shown for several temperatures. At low temperatures, before T = 2.0 the sorption seemed to increase with the temperature; however, above that temperature the sorption curves decayed nearly in a linear way and straight lines were fitted to those data, *i.e.* only the last five data were taken for the fitted line. Similar features were observed for both values of Λ.

In the limit of very strong spring constants, high values of k_B and k_C, the solid particles hardly move from their equilibrium sites, *i.e.* they should remain nearly in the same positions. In the simulations that situation corresponded to the systems with the first model, *i.e.* none harmonic oscillators in the solid particles ($k_B = k_C = 0$). Therefore, regardless of the temperature, sorption curves with high k_C approached the sorption curve with zero spring constant as was expected. In fact, in all cases the chemisorption was always higher for the Einstein solid model than for the rigid solid model.

On the other hand, regardless of the temperature, it was observed that chemisorption increased as the spring constant, k_C, decreased (see Fig. 2) and for a single temperature, the

highest chemisorption was obtained for the lowest k_C value. Those results indicated that the presence of a spring in the solid particles modified the substrate sorption properties. Somehow the springs created fractures in the solid by allowing the gas particles to move deeper into the substrate than those particles that reach other solid particles to interact with them, therefore, more reactions can be produced, *i.e.* more chemisorption is observed. Moreover, from the last model it is possible to test the sorption picture proposed from previous experiments of the reaction $CO_2 + Li_2O \rightleftharpoons Li_2CO_3$ where it was suggested that the solid should crack in order to increase sorption. In our case, cracking was mimicked by the particle vibrations in the solid.

In the same Fig. 2 different slopes for the different k_C curves were observed. In fact, two different states can be characterized (indicated by the different slopes of the fitted straight lines). The first state was described by curves with small k_C (k_C = 0.5 and 1) where the sorption did not change significantly, *i.e.* nearly a zero slope in all the interval of temperatures was observed. The second state was represented by the curves with high k_C where the sorption had significant negative slopes above temperatures $T = 2.5$.

On the other hand, from the same Fig. 2 it was noted that the same chemisorption could be obtained, at different temperatures, by choosing the appropriate spring constant (see Fig. 2). In Fig. 3 plots of k_C as a function of the temperature for a given Λ and for different constant sorption values are shown. Different sorption curves were plotted and it was found that k_C decayed with the temperature. In fact the best fitting curve to the data was the following function,

$$k_C(T) = \frac{1}{a + bT} \tag{11}$$

where "a" and "b" are the fitting parameters for each curve. In all cases the error associated with those fitting parameters are less than 0.1%. The points at low and high temperatures were obtained by extrapolation of the fitted curves in Fig. 2. Therefore, from those data a dependent temperature-spring constant function, $k_C(T)$, was constructed. It is worth mentioning that similar results were obtained if k_C is fixed and k_B is changing.

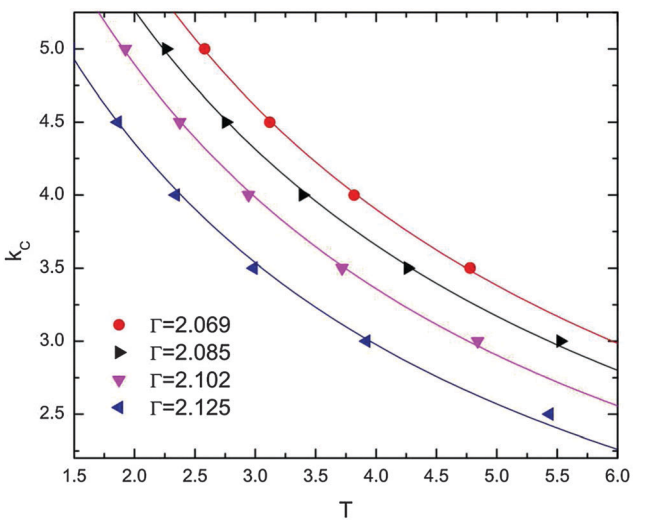

Fig. 3 Spring constants, k_C, as a function of the temperature (with Λ = 0.001) for different sorption values, Γ. The fitting "a" and "b" parameters (in eqn (11)) are 0.09889 and 0.03935 (red circles), 0.10652 and 0.04175 (black triangles), 0.11094 and 0.04668 (pink triangles), 0.12318 and 0.05319 (dark blue triangles), respectively.

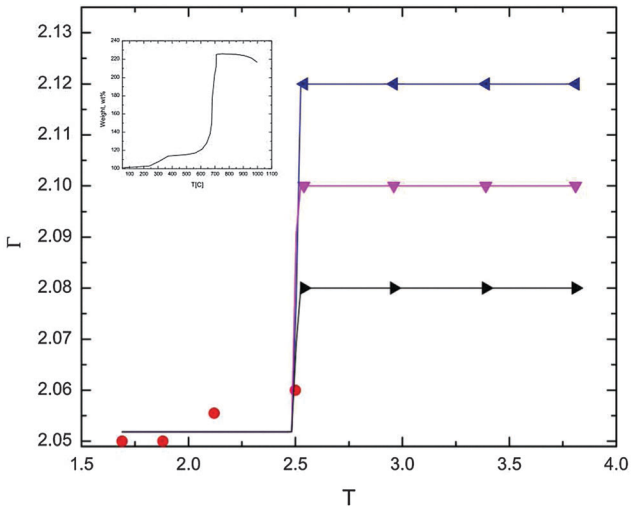

Fig. 4 Sorption curves as a function of the temperature for Λ = 0.001. Simulations were conducted for different $k_C(T)$ with different parameters (in eqn (11)) using the same symbols and colors described in Fig. 3. The lines are given as a guide to the eye only. The experimental results for the chemical reaction $CO_2 + Li_2O \rightleftharpoons Li_2CO_3$ are shown (in real units) in the inset plot taken from ref. 2.

With the previous results another series of computations were conducted using the temperature-spring function (eqn (11)) as an input in the simulations. Moreover, in order to better capture some experimental tendencies two different $k_C(T)$ functions were used in the same simulation; one for temperatures below $T = 2.5$ where a change in the slope was observed as discussed previously, and another for temperatures above that value. In Fig. 4 the results for those simulations at different $k_C(T)$ (by using different parameters) are shown. A nearly constant chemisorption up to a temperature of $T = 2.5$ ($\approx$300 °C) was observed where it reached a higher value, then the sorption decayed slowly with the temperature. Those results showed the same tendencies observed in actual experiments of a similar chemical reaction.[2] Also in Fig. 4 experimental results of the reaction $CO_2 + Li_2O \rightleftharpoons Li_2CO_3$ are shown in real temperature units.

3.2 Structure

The structure of the gas particles "A" can be analyzed in terms of density profiles, $\rho(z)$, calculated along the Z-direction. By looking at those density profiles it was possible to determine how those particles were distributed throughout the simulation box. In Fig. 5 density profiles for the gas particles are shown for the rigid and for the Einstein solid models. Since the profiles next to the walls were symmetric only plots for one solid surface were shown in the figure. In both models not only chemisorption but also physisorption of gas molecules on the surface was observed. Fig. 5a shows a typical density profile of a system

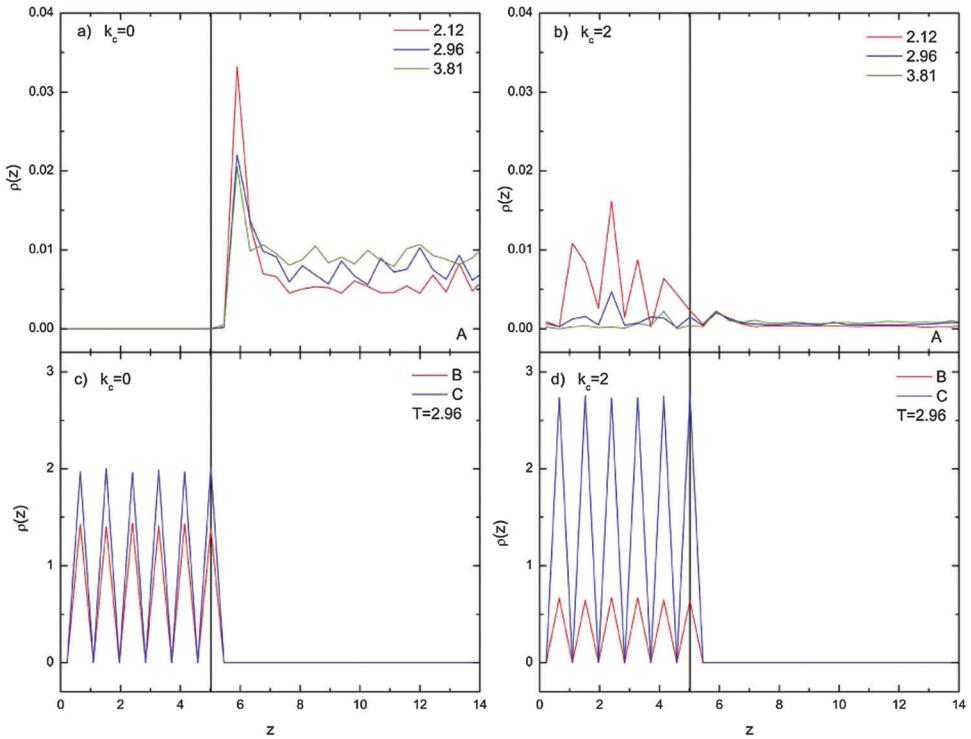

Fig. 5 Typical density profiles at different spring constants. Top plots are for the gas particles (type A) and the bottom for the solid particles "B" and "C". Left plots for the rigid model and right plots for the Einstein solid model. The location of the solid wall is indicated by the black line.

with zero spring constant (rigid model) where physisorption on the solid surfaces was observed indicated by the first high peak close to the walls. Beyond the solid walls a uniform density along the simulation box was observed. Less physisorption was observed as the temperature increased as indicated by the smaller peaks in the density profiles. It was also interesting to observe the density profiles of particles "B" and "C" after the reaction. In all cases those particles were nearly uniformly distributed in the different layers of the solid, however, profiles of particles "B" were lower than the profiles of particles "C" suggesting that the reactions to form particles "C" were more favored.

For the second wall model different issues were observed. For instance, the profiles of the specie "A" showed gas particles inside and outside the walls (Fig. 5b and d). For this model it seemed that oscillations of the solid particles created gaps by allowing the fluid molecules (specie A) to move inside the solid, then sorption was enhanced. These results were in agreement with those of the previous section. Moreover, in this case it was also observed that profiles of particles "B" and "C" were uniformly distributed in the solid and, regardless of the spring constant, there were more particles "C" than particles "B" as indicated by the heights of the profiles, *i.e.* once again sorption of particles "C" was favored. On the other hand, for this model it was depicted that physisorption was lower than for the rigid solid model, *i.e.* the first peak next to the walls for the Einstein solid model was lower than for the first model. In this case the gas density (particles "A") along the simulation box was also lower than for the rigid solid model.

4 Conclusions

Computer simulations to investigate sorption of gases in solid surfaces were conducted using the reactive Monte Carlo method (RxMC). Since the method allows us to work direct chemical reactions it was possible to observe not only physisorption but also chemisorption. In order to reproduce experimental tendencies two simple models were simulated. In the first model the solid was constructed with rigid particles whereas in the second model the particles which formed the solid possessed independent spring constants, *i.e.* an Einstein solid was simulated. Despite being a simple model it presented good agreement with the real reaction $CO_2 + Li_2O \rightleftharpoons Li_2CO_3$. In fact, the second model was built to explain the unusual jump in sorption experiments. Several spring constants were tested and in all cases the sorption was promoted. In contrast to the first model the second model seemed to produce free paths in the solid by allowing the gas particles to move inside to enhance sorption. Moreover, a temperature dependent spring constant function was formulated and it was found to be an inverse function of the spring with the temperature.

Acknowledgements

The authors acknowledge support from Grants DGAPA-UNAM-Mexico IN102812, CONACyT-Mexico 154899 and DGTIC-UNAM for the supercomputer facilities. ML-P acknowledges the post-graduate scholarship from DGAPA-UNAM.

References

1 Z. Qi, H. Daying, L. Yang, Y. Qian and Z. Zibin, *AIChE J.*, 2013, **59**, 901.
2 H. A. Mosqueda, C. Vazquez, P. Bosh and H. Pfeiffer, *Chem. Mater.*, 2006, **18**, 2307.
3 S. Shan, Q. Jia and L. Jiang, *et al.*, *Ceram. Int.*, 2013, **39**, 5437.
4 M. T. Dunstan, W. Liu and A. F. Adriano, *et al.*, *Chem. Mater.*, 2013, **25**, 4881.
5 T. Avalos-Rendon, V. H. Lara and H. Pfiefffer, *Ind. Eng. Chem. Res.*, 2012, **51**, 2622.
6 K. Essaki, K. Nakagawa, M. Kato and H. J. Uemoto, *J. Chem. Eng. Jpn.*, 2004, **37**, 772.
7 B. N. Nair, T. Yamaguchi, H. Kawamura, S. I. Nakao and K. Nakagawa, *J. Am. Ceram. Soc.*, 2004, **87**, 68.
8 B. Zhang, A. C. T. van Duin and J. K. Johnson, *J. Phys. Chem. B*, 2014, **118**, 12008.
9 Y. Duan, K. Zhang and X. S. Li, *et al.*, *Aerosol Air Qual. Res.*, 2014, **14**, 470.
10 L. Yue and W. Lipinski, *Int. J. Heat Mass transfer.*, 2015, **85**, 1058.
11 A. Nalaparaju, M. Khurana and S. Farooq, *et al.*, *Chem. Eng. Sci.*, 2015, **124**, 70.
12 J. Carrero-Mantilla and M. Llano-Restrepo, *Fluid Phase Equilib.*, 2006, **242**, 189.
13 A. A. Sizova, V. V. Sizov and E. N. Brodskaya, *Colloid. J.*, 2015, **77**, 82.
14 Z. Jin and A. Firoozabadi, *Fluid Phase Equilib.*, 2014, **382**, 10.
15 L. Huang, K. L. Joshi and A. C. T. van Duin, *et al.*, *Phys. Chem. Chem. Phys.*, 2012, **14**, 11327.
16 J. C. Palmer, J. D. Moore and T. J. Roussel, *et al.*, *Phys. Chem. Chem. Phys.*, 2011, **13**, 3985.
17 H. Dominguez, *Rev. Mex. Fis.*, 2012, **58**, 378.
18 C. H. Turner, J. K. Brennan, M. Lisal, W. R. Smith, J. K. Johnson and K. E. Gubbins, *Mol. Simul.*, 2008, **34**, 119.
19 K. E. Gubbins, Y.-C. Liu, J. D. Moore and J. C. Palmer, *Phys. Chem. Chem. Phys.*, 2011, **13**, 58.
20 M. Lisal, J. K. Brennan and W. R. Smith, *J. Chem. Phys.*, 2006, **124**, 064712.
21 C. Dapeng and W. Jianzhong, *Carbon*, 2005, **43**, 1364.
22 B. Salah and N. Salah, *J. Mol. Struc.*, 2007, **837**, 206.
23 J. M. Miguez, M. M. Piñeiro and F. J. Blas, *J. Chem. Phys.*, 2013, **138**, 034707.
24 J. K. Johnson, A. Z. Panagiotopoulos and K. E. Gubbins, *Molec. Phys.*, 1994, **81**, 717.
25 M. P. Allen and D. J. Tildesley, *Computer Simulations of Liquids*, Claredon Press, Oxford, 1993.
26 D. A. MacQuarrie, *Statistical Mechanics*, Harper and Row, 1976.
27 J. K. Jonhson, J. A. Zollweg and K. E. Gubbins, *Mol. Phys.*, 1993, **78**, 591.